



Spectral- and size-resolved mass absorption efficiency of mineral dust aerosols in the shortwave spectrum: a simulation chamber study

Lorenzo Caponi^{1,2}, Paola Formenti¹, Dario Massabó², Claudia Di Biagio¹, Mathieu Cazaunau¹, Edouard Pangui¹, Servanne Chevaillier¹, Gautier Landrot³, Meinrat O. Andreae^{4,11}, Konrad Kandler⁵, Stuart Piketh⁶, Thuraya Saeed⁷, Dave Seibert⁸, Earle Williams⁹, Yves Balkanski¹⁰, Paolo Prati², and Jean-François Doussin¹

¹Laboratoire Interuniversitaire des Systèmes Atmosphériques (LISA), UMR CNRS 7583, Université Paris-Est Créteil and Université Paris Diderot, Institut Pierre Simon Laplace, Créteil, France

²Department of Physics & INFN, University of Genoa, Genoa, Italy

³Synchrotron SOLEIL, L'Orme des Merisiers Saint-Aubin, France

⁴Biogeochemistry Department, Max Planck Institute for Chemistry, P.O. Box 3060, 55020 Mainz, Germany

⁵Institut für Angewandte Geowissenschaften, Technische Universität Darmstadt, Schnittspahnstr. 9, 64287 Darmstadt, Germany

⁶Climatology Research Group, University of the Witwatersrand, Johannesburg, South Africa

⁷Science Department, College of Basic Education, Public Authority for Applied Education and Training, Al-Ardiya, Kuwait

⁸Sallyport Global, Phoenix, Arizona, USA

⁹Massachusetts Institute of Technology, Cambridge, Massachusetts, USA

¹⁰LSCE, CNRS UMR8212, CEA, Université de Versailles Saint-Quentin, Gif-sur-Yvette, France

¹¹Geology and Geophysics Department, King Saud University, Riyadh, Saudi Arabia

Correspondence to: Paola Formenti (paola.formenti@lisa.u-pec.fr)

Received: 2 January 2017 – Discussion started: 25 January 2017

Revised: 5 May 2017 – Accepted: 18 May 2017 – Published: 16 June 2017

Abstract. This paper presents new laboratory measurements of the mass absorption efficiency (MAE) between 375 and 850 nm for 12 individual samples of mineral dust from different source areas worldwide and in two size classes: PM_{10.6} (mass fraction of particles of aerodynamic diameter lower than 10.6 μm) and PM_{2.5} (mass fraction of particles of aerodynamic diameter lower than 2.5 μm). The experiments were performed in the CESAM simulation chamber using mineral dust generated from natural parent soils and included optical and gravimetric analyses.

The results show that the MAE values are lower for the PM_{10.6} mass fraction (range 37–135 × 10⁻³ m² g⁻¹ at 375 nm) than for the PM_{2.5} (range 95–711 × 10⁻³ m² g⁻¹ at 375 nm) and decrease with increasing wavelength as λ^{-AAE}, where the Ångström absorption exponent (AAE) averages between 3.3 and 3.5, regardless of size. The size independence of AAE suggests that, for a given size distribution, the

dust composition did not vary with size for this set of samples. Because of its high atmospheric concentration, light absorption by mineral dust can be competitive with black and brown carbon even during atmospheric transport over heavily polluted regions, when dust concentrations are significantly lower than at emission. The AAE values of mineral dust are higher than for black carbon (~1) but in the same range as light-absorbing organic (brown) carbon. As a result, depending on the environment, there can be some ambiguity in apportioning the aerosol absorption optical depth (AAOD) based on spectral dependence, which is relevant to the development of remote sensing of light-absorbing aerosols and their assimilation in climate models. We suggest that the sample-to-sample variability in our dataset of MAE values is related to regional differences in the mineralogical composition of the parent soils. Particularly in the PM_{2.5} fraction, we found a strong linear correlation between the dust light-

absorption properties and elemental iron rather than the iron oxide fraction, which could ease the application and the validation of climate models that now start to include the representation of the dust composition, as well as for remote sensing of dust absorption in the UV–vis spectral region.

1 Introduction

Mineral dust aerosols emitted by wind erosion of arid and semiarid soils account for about 40 % of the total emitted aerosol mass per year at the global scale (Knippertz and Stuut, 2014). The episodic but frequent transport of intense mineral dust plumes is visible from spaceborne sensors because their high concentrations, combined with their ability to scatter and absorb solar and thermal radiation, give rise to the highest registered values of aerosol optical depth (AOD) on Earth (Chiapello, 2014). The instantaneous radiative efficiency of dust particles, that is, their radiative effect per unit AOD, is of the order of tens to hundreds of $\text{W m}^{-2} \text{AOD}^{-1}$ in the solar spectrum and of the order of tens of $\text{W m}^{-2} \text{AOD}^{-1}$ in the thermal infrared (e.g., Haywood et al., 2003; di Sarra et al., 2011; Slingo et al., 2006; and the compilation of Highwood and Ryder, 2014). Albeit partially compensated by the radiative effect in the thermal infrared, the global mean radiative effect of mineral dust in the shortwave is negative both at the surface and the top of the atmosphere (TOA) and produces a local warming of the atmosphere (Boucher et al., 2013). There are numerous impacts of dust on global and regional climate, which ultimately feed back on wind speed and vegetation and therefore on dust emission (Tegen and Lacis, 1996; Solmon et al., 2008; Pérez et al., 2006; Miller et al., 2014). Dust particles perturb the surface air temperature through their radiative effect at TOA, can increase the atmospheric stability (e.g., Zhao et al., 2011) and might affect precipitation at the global and regional scale (Solmon et al., 2008; Xian, 2008; Vinoj et al., 2014; Miller et al., 2014, and references therein).

All models indicate that the effect of mineral dust on climate has great sensitivity to their shortwave absorption properties (Miller et al., 2004; Lau et al., 2009; Loeb and Su, 2010; Ming et al., 2010; Perlwitz and Miller, 2010). Absorption by mineral dust started receiving a great deal of interest when spaceborne and ground-based remote-sensing studies (Dubovik et al., 2002; Colarco et al., 2002; Sinyuk et al., 2003) suggested that mineral dust was less absorbing than had been suggested by in situ observations (e.g., Patterson et al., 1977; Haywood et al., 2001), particularly at wavelengths below 600 nm. Balkanski et al. (2007) showed that lowering the dust absorption properties to an extent that reconciles them both with the remote-sensing observations and the state of knowledge of the mineralogical composition allowed calculating the clear-sky shortwave radiative effect of dust in agreement with satellite-based observations. A significant

number of observations have quantified the shortwave light-absorbing properties of mineral dust both by direct measurements (Alfaro et al., 2004; Linke et al., 2006; Osborne et al., 2008; McConnell et al., 2008; Derimian et al., 2008; Yang et al., 2009; Müller et al., 2009; Petzold et al., 2009; Formenti et al., 2011; Moosmüller et al., 2012; Wagner et al., 2012; Ryder et al., 2013a; Utry et al., 2014; Denjean et al., 2016a, b) and indirectly by quantifying the amount and the speciation of the light-absorbing compounds in mineral dust, principally iron oxides (Lafon et al., 2004, 2006; Lazaro et al., 2008; Derimian et al., 2008; Zhang et al., 2008; Kandler et al., 2007, 2009, 2011; Formenti et al., 2014a, b).

However, existing data are often limited to a single wavelength, which moreover is not the same for all experiments. Also, frequently they do not represent the possible regional variability of the dust absorption, either because they are obtained from field measurements integrating the contributions of different source regions or, conversely, by laboratory investigations targeting samples from a limited number of locations. This might lead to biases in the data. Indeed, iron oxides in mineral dust, mostly in the form of hematite (Fe_2O_3) and goethite ($\text{Fe}(\text{O})\text{OH}$), have specific absorption bands in the UV–vis spectrum (Bédidi and Cervelle, 1993) and have a variable content depending on the soil mineralogy of the source regions (Journet et al., 2014).

In this study, experiments on 12 aerosol samples generated from natural parent top soils from various source regions worldwide were conducted with a large atmospheric simulation chamber. We present a new evaluation of the ultraviolet to near-infrared (375–850 nm) light-absorbing properties of mineral dust by investigating the size-segregated mass absorption efficiency (MAE, units of $\text{m}^2 \text{g}^{-1}$) and its spectral dependence, widely used in climate models to calculate the direct radiative effect of aerosols.

2 Instruments and methods

At a given wavelength, λ , MAE is defined as the ratio of the aerosol light-absorption coefficient $b_{\text{abs}}(\lambda)$ (units of m^{-1}) and its mass concentration (in $\mu\text{g m}^{-3}$):

$$\text{MAE}(\lambda) = \frac{b_{\text{abs}}(\lambda)}{\text{mass concentration}}. \quad (1)$$

MAE values for mineral dust aerosol are expressed in $10^{-3} \text{m}^2 \text{g}^{-1}$. The spectral dependence of the aerosol absorption coefficient $b_{\text{abs}}(\lambda)$ is described by the power-law relationship

$$b_{\text{abs}}(\lambda) \sim \lambda^{-\text{AAE}}, \quad (2)$$

where the AAE is the Ångström absorption exponent, representing the negative slope of $b_{\text{abs}}(\lambda)$ in a log–log plot (Moosmüller et al., 2009):

$$\text{AAE} = -\frac{d \ln(b_{\text{abs}}(\lambda))}{d \ln(\lambda)}. \quad (3)$$

2.1 The CESAM (Experimental Multiphase Atmospheric Simulation Chamber)

The experiments in this work have been performed in the 4.2 m³ stainless-steel CESAM (Wang et al., 2011). The CESAM has been extensively used in recent years to simulate, at sub- and super-saturated conditions, the formation and properties of aerosols at concentration levels comparable to those encountered in the atmosphere (Denjean et al., 2015a, b; Brégonzio-Rozier et al., 2015, 2016; Di Biagio et al., 2014, 2017).

CESAM is a multi-instrumented platform, equipped with 12 circular flanges to support its analytical environment. Basic instrumentation comprises sensors to measure the temperature, pressure and relative humidity within the chamber (two manometers MKS Baratron[®] (622A and 626A) and a HMP234 Vaisala[®] humidity and temperature sensor). The particle size distribution is routinely measured by a combination of (i) a scanning mobility particle sizer (SMPS, mobility diameter range 0.02–0.88 μm), composed of a differential mobility analyzer (DMA, TSI Inc. model 3080) and a condensation particle counter (CPC, TSI Inc. model 3772); (ii) a SkyGrimm optical particle counter (Grimm Inc., model 1.129, optical equivalent diameter range 0.25–32 μm); and (iii) a WELAS optical particle counter (PALAS, model 2000, optical equivalent diameter range 0.5–47 μm). Full details of operations and data treatment of the particle counters are provided in Di Biagio et al. (2017).

2.2 Filter sampling

Three filter samples per top-soil sample were collected on different types of substrate based on the analysis to be performed. Sampling dedicated to the determination of the aerosol mass concentration by gravimetric analysis and the measurement of the absorption coefficients by optical analysis was performed on 47 mm quartz membranes (Pall Tissuquartz[™], 2500 QAT-UP). Two samples were collected in parallel. The first quartz membrane sample (“total”) was collected without a dedicated size cutoff using an in-house-built stainless-steel sampler operated at 5 L min⁻¹. However, as detailed in Di Biagio et al. (2017), the length of the sampling line from the intake point in the chamber to the filter entrance was 50 cm, resulting in a 50 % cutoff of the transmission efficiency at 10.6 μm particle aerodynamic diameter. This fraction is therefore indicated as PM_{10.6} in the following discussion. The second quartz membrane sample was collected using a four-stage DEKATI impactor operated at a flow rate of 10 L min⁻¹ to select the aerosol fraction of particles with aerodynamic diameter smaller than 2.5 μm, indicated as PM_{2.5}. Sampling for the analysis of the iron oxide content was performed on polycarbonate filters (47 mm Nuclepore, Whatman; pore size 0.4 μm) using the same sample holder as used for the total quartz filters and therefore corresponding to the PM_{10.6} mass fraction. Samples were col-

lected at a flow rate of 6 L min⁻¹. All flow rates were monitored by a thermal mass flowmeter (TSI Inc., model 4140). These samples were also used to determine the elemental composition (including Fe) and the fraction of iron oxides in the total mass.

2.3 The multi-wavelength absorbance analyzer (MWAA)

The aerosol absorption coefficient, $b_{\text{abs}}(\lambda)$, at five wavelengths ($\lambda = 375, 407, 532, 635$ and 850 nm) was measured by in situ analysis of the quartz filter samples using the MWAA, described in detail in Massabò et al. (2013, 2015).

The MWAA performs a nondestructive scan of the quartz filters at 64 different points, each ~ 1 mm² wide. It measures the light transmission through the filter as well as backscattering at two different angles (125 and 165°). This is necessary to constrain the multiple scattering effects occurring within the particle-filter system. The measurements are used as input to a radiative transfer model (Hänel, 1987, 1994) as implemented by Petzold and Schönlinner (2004) for the multi-angle absorption photometry (MAAP) measurements. In this model, a two-stream approximation is applied (Coakley and Chylek, 1975), in which the fractions of hemispherical backscattered radiation with respect to the total scattering for collimated and diffuse incident radiation are approximated on the basis of the Henyey–Greenstein scattering phase function (Hänel, 1987). This approximation assumes a wavelength-independent asymmetry parameter (g) set to 0.75, appropriate for mineral dust (Formenti et al., 2011; Ryder et al., 2013b). The total uncertainty, including the effects of photon counting and the deposit inhomogeneity, on the absorption coefficient measurement is estimated at 8 % (Petzold and Schönlinner, 2004; Massabò et al., 2013).

2.4 Gravimetric analysis

The aerosol mass deposited on the filters (μg) was obtained by weighing the quartz filter before and after sampling, after a period of 48 h of conditioning in a room with controlled atmospheric conditions (temperature $\sim 20 \pm 1$ °C; relative humidity $\sim 50 \pm 5$ %). Weighing is performed with an analytical balance (Sartorius model MC5, precision of 1 μg) and repeated three times to control the statistical variability of the measurement. Electrostatic effects are removed by exposing the filters, prior weighing, to a de-ionizer. The error in the measured mass is estimated at 1 μg, including the repetition variability. The aerosol mass concentration (μg m⁻³) is obtained by dividing the mass deposited on the filter to the total volume of sampled air (m³) obtained from the mass flowmeter measurements (± 5 %). The percent error on mass concentrations is estimated to 5 %.

Table 1. Characteristics of the standards used for the quantification of the iron oxides in the XAS analysis.

Standard	Stoichiometric formula	Origin
Illite of Puy	(Si _{3.55} Al _{0.45})(Al _{1.27} Fe _{0.36} Mg _{0.44})O ₁₀ (OH) ₂ (Ca _{0.01} Na _{0.01} K _{0.53} X(I) _{0.12})	Puy, France
Goethite	FeO OH	Minnesota
Hematite	Fe ₂ O ₃	Niger
Montmorillonite	(Na,Ca) _{0,3} (Al,Mg) ₂ Si ₄ O ₁₀ (OH) ₂ · n(H ₂ O)	Wyoming
Nontronite	Na _{0,3} Fe ₂ (Si,Al) ₄ O ₁₀ (OH) ₂ · nH ₂ O	Pennsylvania

2.5 Dust composition measurements

2.5.1 Elemental composition

Elemental concentrations for the major constituents of mineral dust (Na, Mg, Al, Si, P, S, Cl, K, Ca, Fe, Ti, Mn) were obtained by wavelength-dispersive X-ray fluorescence (WD-XRF) of the Nuclepore filters using a PW-2404 spectrometer by Panalytical. Excitation X-rays are produced by a Coolidge tube ($I_{\max} = 125$ mA, $V_{\max} = 60$ kV) with an Rh anode; the primary X-ray spectrum can be controlled by inserting filters (Al, at different thickness) between the anode and the sample. Each element was analyzed three times, with specific conditions (voltage, tube filter, collimator, analyzing crystal and detector). Data collection was controlled by the SuperQ software provided with the instrument. The elemental mass thickness ($\mu\text{g cm}^{-2}$), that is, the analyzed elemental mass per unit surface, was obtained by comparing the elemental yields with a sensitivity curve measured in the same geometry on a set of certified mono- or bi-elemental thin layer standards by Micromatter Inc. The certified uncertainty of the standard deposit ($\pm 5\%$) determines the lower limit of the uncertainty of the measured elemental concentrations, which ranges between 8 and 10 % depending on the element considered. Thanks to the uniformity of the aerosol deposit on the filters, the atmospheric elemental concentrations ($\mu\text{g m}^{-3}$) were calculated by multiplying the analyzed elemental mass thickness by the ratio between the collection and analyzed surfaces of each sample (41 and 22 mm, respectively), then dividing by the total sampled volume (m^3). Finally, concentrations of light-weight elements (atomic number $Z < 19$) were corrected for the underestimation induced by the self-absorption of the emitted soft X-rays inside aerosol particles according to Formenti et al. (2010).

Additional XRF analysis of the quartz filters was performed both in the PM_{10.6} and the PM_{2.5} fractions to verify the absence of biases between the experiments dedicated to the determination of particle composition and those where the optical properties were measured.

2.5.2 Iron oxide content

The content and the mineralogical speciation of the iron oxides, also defined as free iron, i.e., the fraction of iron that is not in the crystal lattice of silicates (Karickhoff and Bai-

ley, 1973), was determined by XANES (X-ray absorption near-edge structure) in the Fe K-range (K_{α} , 7112 eV) at the SAMBA (Spectroscopies Applied to Materials based on Absorption) beamline at the SOLEIL synchrotron facility in Saclay, France (Brioso et al., 2011). The position and shape of the K pre-edge and edge peaks were analyzed as they depend on the oxidation state of iron and the atomic positions of the neighboring ions, mostly O⁺ and OH⁻.

As in Formenti et al. (2014b), samples were mounted in an external setup mode. A Si(220) double-crystal monochromator was used to produce a monochromatic X-ray beam, which was $3000 \times 250 \mu\text{m}^2$ in size at the focal point. The energy range was scanned from 6850 to 7800 eV at a step resolution varying between 0.2 eV in proximity to the Fe K absorption edge (at 7112 eV) to 2 eV in the extended range. Samples were analyzed in fluorescence mode without prior preparation. One scan acquisition lasted approximately 30 min and was repeated three times to improve the signal-to-noise ratio.

The same analytical protocol was applied to five standards of Fe(III)-bearing minerals (Table 1), including iron oxides (hematite, goethite) and silicates (illite, montmorillonite, nontronite). The standard spectra were used to deconvolute the dust sample spectra to quantify the mineralogical status of iron. The linear deconvolution was performed with the Athena IFEFFIT freeware analysis program (Ravel and Newville, 2005). This provided the proportionality factors, α_i , representing the mass fraction of elemental iron to be assigned to the i th standard mineral. In particular, the values of α_{hem} and α_{goe} represent the mass fractions of elemental iron that can be attributed to hematite and goethite, and $\alpha_{\text{Fe ox}}$ ($\alpha_{\text{hem}} + \alpha_{\text{goe}}$) is the mass fraction of elemental iron that can be attributed to iron oxides.

2.5.3 Calculation of the iron oxide content

The measured elemental concentrations obtained by XRF are expressed in the form of elemental oxides and summed to estimate the total mineral dust mass concentration MC_{dust} according to the equation from Lide (1992):

$$[\text{MC}_{\text{dust}}] = 1.12 \times \left\{ 1.658[\text{Mg}] + 1.889[\text{Al}] + 2.139[\text{Si}] + 1.399[\text{Ca}] + 1.668[\text{Ti}] + 1.582[\text{Mn}] \right\} + (0.5 \times 1.286 + 0.5 \times 1.429 + 0.47 \times 1.204)[\text{Fe}] \quad (4)$$

The relative uncertainty in MC_{dust} , estimated from the analytical error in the measured concentrations, does not exceed

6 %. As it will be explained in the Results section (Sect. 3.1), the values of MC_{dust} estimated from Eq. (4) were found in excellent agreement with the measured gravimetric mass on the filters.

The fractional mass ratio (in %) of elemental iron ($MR_{\text{Fe}\%}$) with respect to the total dust mass concentration, MC_{dust} , is then calculated as

$$MR_{\text{Fe}\%} = \frac{[\text{Fe}]}{[MC_{\text{dust}}]} \times 100. \quad (5)$$

The mass concentration of iron oxides or free iron ($MC_{\text{Fe ox}}$), representing the fraction of elemental iron in the form of hematite and goethite (Fe_2O_3 and FeOOH , respectively), is equal to

$$MC_{\text{Fe ox}} = MC_{\text{hem}} + MC_{\text{goe}}, \quad (6)$$

where MC_{hem} and MC_{goe} are the total masses of hematite and goethite. These can be calculated from the values α_{hem} and α_{goe} from XANES analysis, which represent the mass fractions of elemental iron attributed to hematite and goethite, as

$$MC_{\text{hem}} = \frac{\alpha_{\text{hem}} \times [\text{Fe}]}{0.70}, \quad (7)$$

$$MC_{\text{goe}} = \frac{\alpha_{\text{goe}} \times [\text{Fe}]}{0.63}, \quad (8)$$

where the values of 0.70 and 0.63 represent the mass molar fractions of Fe in hematite and goethite, respectively. The relative errors of MC_{hem} and MC_{goe} are obtained from the uncertainties of the values of α_{hem} and α_{goe} from XANES analysis (less than 10 %).

The mass ratio of iron oxides ($MR_{\text{Fe ox}\%}$) with respect to the total dust mass can then be calculated as

$$MR_{\text{Fe ox}\%} = MC_{\text{Fe ox}} \times MR_{\text{Fe}\%}. \quad (9)$$

3 Experimental protocol

At the beginning of each experiment, the chamber was evacuated to 10^{-4} – 10^{-5} hPa. Then, the reactor was filled with a mixture of 80 % N_2 and 20 % O_2 at a pressure slightly exceeding the current atmospheric pressure, in order to avoid contamination from ambient air. The experiments were conducted at ambient temperature and at a relative humidity < 2 %. As in Di Biagio et al. (2014, 2017), dust aerosols were generated by mechanical shaking of the parent soils, previously sieved to < 1000 μm and dried at 100 °C for about 1 h to remove any residual humidity. About 15 g of soil was placed in a Buchner flask and shaken for about 30 min at 100 Hz by means of a sieve shaker (Retsch AS200). The dust particles produced by the mechanical shaking, mimicking the saltation processing that soils experience when eroded by strong winds, were injected in the chamber by flushing the

flask with N_2 at 10 L min^{-1} for about 10–15 min, whilst continuing shaking the soil. Di Biagio et al. (2014, 2017) demonstrated the realism of the generation system concerning the composition and the size distribution of the generated dust with respect to the properties of mineral dust in the atmosphere.

The dust remained suspended in the chamber for approximately 120 min thanks to the four-wheel fan located in the bottom of the chamber body. Previous measurements at the top and bottom of the chamber showed that the fan ensures a homogeneous distribution of the dust starting approximately 10 min after the end of the injection (Di Biagio et al., 2014).

To compensate for the air extracted from the chamber by sampling, a particle-free flow of N_2/O_2 , regulated in real time as a function of the total volume of sampled air, was re-injected in the chamber. To avoid excessive dilution the flow was limited to 20 L min^{-1} . Two experiments per soil type were conducted: a first experiment for sampling on the Nuclepore polycarbonate filters (determination of the elemental composition and the iron oxide fraction) and in situ measurements of the infrared optical constants (Di Biagio et al., 2017), and a second experiment sampling on total quartz filter and impactor for the study of dust MAE presented in this paper.

Figure 1 illustrates as typical example the time series of the aerosol mass concentration during the two experiments conducted for the Libyan sample. The comparison demonstrates the repeatability of the dust concentrations, both in absolute values and in temporal dynamics. It also shows that the mass concentrations decreased very rapidly by gravitational settling within the first 30 min of the experiment (see also the discussion in Di Biagio et al., 2017), after which concentrations only decrease by dilution. The filter sampling was started after this transient phase, and then continued through the end of the experiments, in order to collect enough dust on the filter membranes for subsequent chemical analysis. Blank samples were collected before the start of the experiments by placing the holders loaded with filter membranes in line with the chamber and by flushing them for a few seconds with air coming from the chamber.

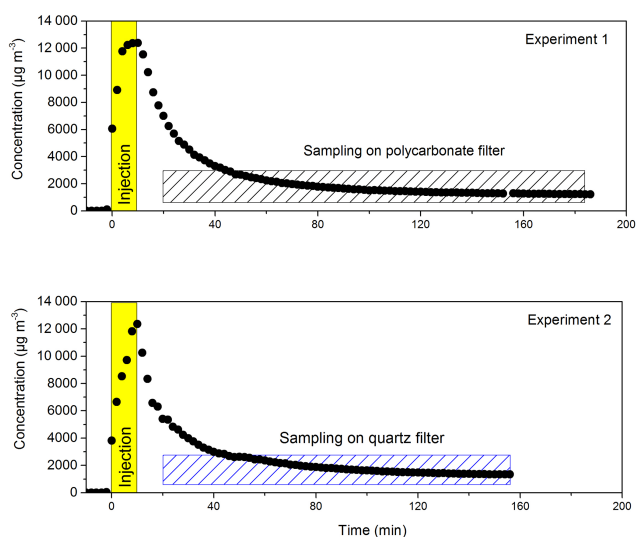
At the end of each experimental series with a given soil sample, the chamber was manually cleaned in order to remove carry-over caused by resuspension of particles deposited to the walls. Background concentrations of aerosols in the chamber vary between 0.5 and 2.0 $\mu\text{g m}^{-3}$, i.e., a factor of 500 to 1000 below the operating conditions.

4 Results and discussion

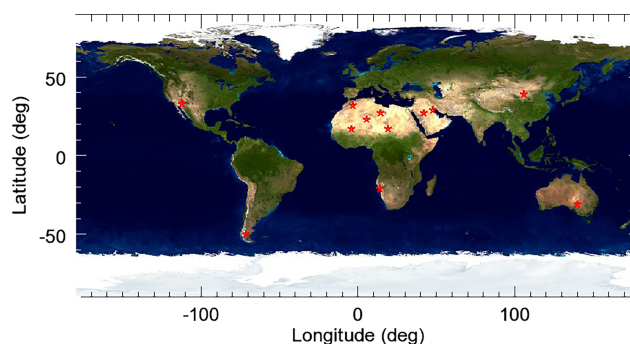
The geographical location of the soil collection sites is shown in Fig. 2, and the coordinates are summarized in Table 2. The selection of these soils and sediments was made out of 137 individual top-soil samples collected in major arid and semiarid regions worldwide and representing the mineralog-

Table 2. Geographical information on the soil samples used in this work.

Geographical area	Sample	Desert area	Geographical coordinates
Sahara	Morocco	East of Ksar Sahli	31.97° N, 3.28° W
	Libya	Sebha	27.01° N, 14.50° E
	Algeria	Ti-n-Tekraouit	23.95° NN, 5.47° E
Sahel	Mali	Dar el Beida	17.62° N, 4.29° W
	Bodélé	Bodélé depression	17.23° N, 19.03° E
Middle East	Saudi Arabia	Nefud	27.49° N, 41.98° E
	Kuwait	Kuwaiti	29.42° N, 47.69° E
Southern Africa	Namibia	Namib	21.24° S, 14.99° E
Eastern Asia	China	Gobi	39.43° N, 105.67° E
North America	Arizona	Sonoran	33.15° N, 112.08° W
South America	Patagonia	Patagonia	50.26° S, 71.50° W
Australia	Australia	Strzelecki	31.33° S, 140.33° E

**Figure 1.** Time series of aerosol mass concentration in the chamber for two companion experiments (Libyan dust). Experiment 1 (top panel) was dedicated to the determination of the chemical composition (including iron oxides) by sampling on polycarbonate filters. Experiment 2 (bottom panel) was dedicated to the determination of the absorption optical properties by sampling on quartz filters.

ical diversity of the soil composition at the global scale. As discussed in Di Biagio et al. (2017), this large sample set was reduced to a set of 19 samples representing the mineralogical diversity of the soil composition at the global scale and based on their availability in sufficient quantities for injection in the chamber. Because some of the experiments did not produce enough dust to perform good-quality optical measurements, in this paper we present a set of 12 samples distributed worldwide but mostly from northern and western Africa (Libya,

**Figure 2.** Locations (red stars) of the soil and sediment samples used to generate dust aerosols.

Algeria, Mali, Bodélé) and the Middle East (Saudi Arabia and Kuwait). Individual samples from the Gobi in Eastern Asia, the Namib, the Strzelecki desert in Australia, the Patagonian Desert in South America and the Sonoran Desert in Arizona were also investigated.

4.1 Elemental composition and iron oxide content

A total of 41 filters including 15 polycarbonate filters (12 samples and 3 blanks) and 25 quartz filters (12 for the total fraction, 10 for the fine fraction and 3 blanks) were collected for analysis. The dust mass concentration found by gravimetric analysis varied between 50 and $5 \mu\text{g m}^{-3}$, in relatively good agreement with the dust mass concentrations, MC_{dust} , from Eq. (4), based on XRF analysis: the slope of the linear regression between the calculated and the gravimetric values of MC_{dust} is 0.90 with $R^2 = 0.86$. Di Biagio et al. (2017) showed that clays are the most abundant mineral phases, together with quartz and calcite, and that sig-

Table 3. Chemical characterization of the dust aerosols in PM_{10.6} and PM_{2.5} (in parentheses) size fractions. Columns 3 and 4 give the Si / Al and Fe / Ca elemental ratios obtained from X-ray fluorescence analysis. The uncertainty of each individual value is estimated to be 10 %. Column 5 shows MC_{Fe%}, the fractional mass of elemental iron with respect to the total dust mass concentration (uncertainty 10 %). Column 6 reports MC_{Fe ox%}, the mass fraction of iron oxides with respect to the total dust mass concentration (uncertainty 15 %). For PM_{2.5} the determination of the Si / Al ratio is impossible due to the composition of the filter membranes (quartz).

Geographical area	Sample	Si / Al	Fe / Ca	MC _{Fe%}	MC _{Fe ox%}
Sahara	Morocco	3.12 (–)	0.24 (0.28)	3.6 (4.4)	1.4 (1.8)
	Libya	2.11 (–)	1.19 (1.12)	5.2 (5.6)	3.1 (3.4)
	Algeria	2.51 (–)	3.14 (4.19)	6.6 (5.4)	2.7 (2.2)
Sahel	Mali	3.03 (–)	2.99 (3.67)	6.6 (33.6)	3.7 (18.7)
	Bodélé	5.65 (–)	12.35 (–)	4.1 (–)	0.7 (–)
Middle East	Saudi Arabia	2.95 (–)	0.29 (0.27)	3.8 (5.1)	2.6 (3.5)
	Kuwait	3.15 (–)	0.89 (1.0)	5.0 (13.6)	1.5 (4.2)
Southern Africa	Namibia	3.41 (–)	0.11 (0.10)	2.4 (6.9)	1.1 (3.1)
Eastern Asia	China	2.68 (–)	0.77 (0.71)	5.8 (13.6)	0.9 (2.5)
North America	Arizona	3.30 (–)	0.95 (–)	5.3 (–)	1.5 (–)
South America	Patagonia	4.80 (–)	4.68 (4.64)	5.1 (–)	1.5 (–)
Australia	Australia	2.65 (–)	5.46 (4.86)	7.2 (11.8)	3.6 (5.9)

nificant variability exists as function of the compositional heterogeneity of the parent soils. Here we use the Fe / Ca and Si / Al elemental ratios obtained from XRF analysis to discriminate the origin of dust samples. These ratios have been extensively used in the past to discriminate the origin of African dust samples collected in the field (Chiapello et al., 1997; Formenti et al., 2011, 2014a). The values obtained during our experiments are reported in Table 3. There is a very good correspondence between the values obtained for the Mali, Libya, Algeria and (to a lesser extent) Morocco experiments to values found in environmental aerosol samples by Chiapello et al. (1997) and Formenti et al. (2011, 2014a). These authors indicate that dust from local erosion of Sahelian soils, such as from Mali, has Si / Al ratios in the range of 2–2.5 and Fe / Ca ratios in the range of 3–20, depending on the time proximity to the erosion event. Dust from sources in the Sahara, such as Libya and Algeria, shows Si / Al ratios in the range of 2–3 and Fe / Ca ratios in the range of 0.7–3, whereas dust from Morocco has Si / Al ratios around 3 and Fe / Ca ratios around 0.4. The only major difference is observed for the Bodélé experiment, for which the Fe / Ca ratio is enriched by a factor of 6 with respect to the values of 1 found during the field observations (Formenti et al., 2011, 2014a). This could reflect the fact that the Bodélé aerosol in the chamber is generated from a sediment sample and not from a soil. As a matter of fact, the Bodélé sediment sample consists of a very fine powder which becomes very easily airborne. This powder is likely to be injected in the chamber with little or no size fractionation. Hence, the aerosol generated from it should have a closer composition to the orig-

inal powder than the other samples. In contrast, Bristow et al. (2010) and Moskowitz et al. (2016) showed that the iron content and speciation of the Bodélé sediments is very heterogeneous at the source scale. For samples from areas other than northern Africa, the largest variability is observed for the Fe / Ca values, ranging from 0.1 to 8, whereas the Si / Al ratio varied only between 2.5 and 4.8. In this case, values are available in the literature for comparison (e.g., Cornille et al., 1990; Reid et al., 1994; Eltayeb et al., 2001; Lafon et al., 2006; Shen et al., 2007; Radhi et al., 2010, 2011; Formenti et al., 2011, 2014a; Scheuvsens et al., 2013, and references within). Values in the PM_{2.5} fraction are very consistent with those obtained in the PM_{10.6}; their linear correlation has a slope of 1.03 (± 0.05) and a R^2 equal to 0.97, suggesting that the elemental composition is relatively size independent.

The mass fraction of total Fe (MC_{Fe%} from Eq. 5), also reported in Table 3, ranged from 2.8 % (Namibia) to 7.3 % (Australia). These are in the range of values reported in the literature, taking into account that differences might be also due to the method (direct measurement/calculation) and/or the size fraction over which the total dust mass concentration is estimated (Chiapello et al., 1997; Reid et al., 1994; 2003; Derimian et al., 2008; Formenti et al., 2001, 2011, 2014a; Scheuvsens et al., 2013). The agreement of MC_{Fe%} values obtained by the XRF analysis of polycarbonate filters (Eq. 5) and those obtained from the XRF analysis of the quartz filters, normalized to the measured gravimetric mass, is well within 10 % (the percent error of each estimate). Exceptions are the samples from Bodélé and Algeria, for which the values obtained from the analysis of the

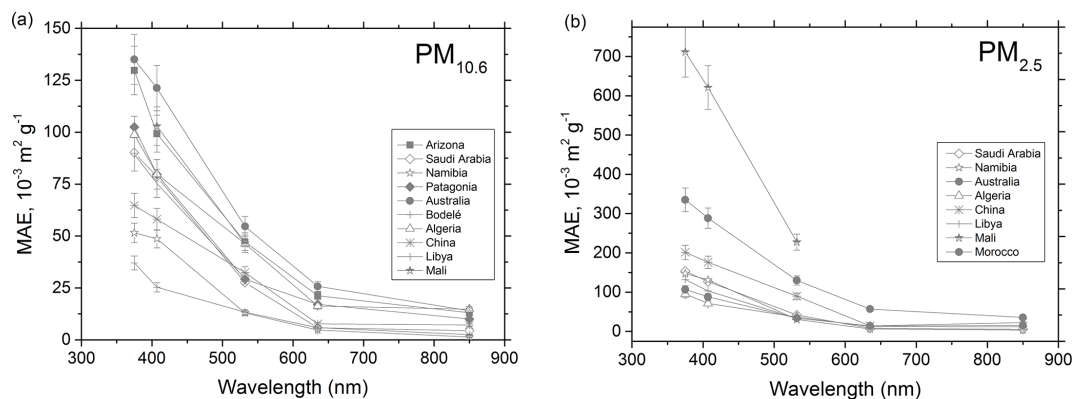


Figure 3. Spectral dependence of the MAE values for the samples investigated in this study in the $\text{PM}_{10.6}$ (a) and in the $\text{PM}_{2.5}$ (b) mass fractions.

quartz filters are significantly lower than those obtained from the Nuclepore filters (3.1 % vs. 4.1 % for Bodélé and 4.3 % vs. 6.8 % for Algeria). We treat that as an additional source of error in the rest of the analysis and add it to the total uncertainty. In the $\text{PM}_{2.5}$ fraction, the content of iron is more variable, ranging from 4.4 % (Morocco) to 33.6 % (Mali), showing a size dependence. A word of caution to this conclusion is that the two estimates are not necessarily consistent in the way that the total dust mass is estimated (from Eq. 4 for the $\text{PM}_{10.6}$ fraction and by gravimetric weighing for the $\text{PM}_{2.5}$).

Finally, between 11 and 47 % of iron in the samples can be attributed to iron oxides, in variable proportions between hematite and goethite. The iron oxide fraction of total Fe in this study is at the lower end of the range (36–72 %) estimated for field dust samples of Saharan/Sahelian origin (Formenti et al., 2014b). The highest value of Formenti et al. (2014b), obtained for a sample of locally emitted dust collected at the Banizoumbou station in the African Sahel, is anyhow in excellent agreement with the value of 62 % obtained for an experiment (not shown here) using a soil collected in the same area. Likewise, the proportions between hematite and goethite (not shown) are reproduced, showing that goethite is more abundant than hematite. The mass fraction of iron oxides ($\text{MR}_{\text{Fe ox\%}}$), estimated from Eq. (8) and shown in Table 3, ranges between 0.7 % (Kuwait) and 3.6 % (Australia), which is in the range of available field estimates (Formenti et al., 2014a; Moskowitz et al., 2016). For China, our value of $\text{MR}_{\text{Fe ox\%}}$ is lower by almost a factor of 3 compared to that obtained for dust of the same origin by Alfaro et al. (2004) (0.9 % against 2.8 %), whereas for a sample from Niger (not considered in this study) our estimates and that by Alfaro et al. (2004) agree perfectly (5.8 %). A possible underestimate of the iron oxide fraction for samples other than those from the Sahara–Sahel area could be due to the fact that – opposite to the experience of Formenti et al. (2014b) – the linear deconvolutions of the XANES spectra were not always satisfactory (see Fig. S1 in the Supplement). This resulted in a significant residual between the observed

and fitted XANES spectra. In fact, the mineralogical reference for hematite is obtained from a soil from Niger (Table 1) and might not be fully suitable for representing aerosols of different origins. Additional differences could arise from differences in the size distributions of the generated aerosol. As a matter of fact, the number fraction of particles in the size classes above $0.5 \mu\text{m}$ in diameter is different in the dust aerosol generated in the Alfaro et al. (2004) study compared to ours. In the study by Alfaro et al. (2004), the number fraction of particles is lowest in the $0.5\text{--}0.7 \mu\text{m}$ size class and highest between 1 and $5 \mu\text{m}$. In contrast, in our study the number fraction is lowest in the $1\text{--}2 \mu\text{m}$ size range and highest between 0.5 and $0.7 \mu\text{m}$. These differences could be due to differences either in the chemical composition or in the total mass in the denominator of Eq. (8).

4.2 Spectral and size variability of the mass absorption efficiency

The spectral MAEs at 375, 407, 532, 635 and 850 nm for the $\text{PM}_{10.6}$ and the $\text{PM}_{2.5}$ dust fractions are summarized in Table 4 and displayed in Fig. 3. Regardless of particle size, the MAE values decrease with increasing wavelength (almost 1 order of magnitude between 375 and 850 nm) and display a larger variability at shorter wavelengths. The MAE values for the $\text{PM}_{10.6}$ range from $37 (\pm 3) \times 10^{-3}$ to $135 (\pm 11) \times 10^{-3} \text{m}^2 \text{g}^{-1}$ at 375 nm and from $1.3 (\pm 0.1) \times 10^{-3}$ to $15 (\pm 1) \times 10^{-3} \text{m}^2 \text{g}^{-1}$ at 850 nm. Maxima are found for the Australia and Algeria samples, whereas the minima are for Bodélé and Namibia at, respectively, 375 and 850 nm. In the $\text{PM}_{2.5}$ fraction, the MAE values range from $95 (\pm 8) \times 10^{-3}$ to $711 (\pm 70) \times 10^{-3} \text{m}^2 \text{g}^{-1}$ at 375 nm and from $3.2 (\pm 0.3) \times 10^{-3}$ to $36 (\pm 3) \times 10^{-3} \text{m}^2 \text{g}^{-1}$ at 850 nm. Maxima at both 375 and 850 nm are found for the Morocco sample, whereas the minima are for Algeria and Namibia, respectively. The MAE values for mineral dust resulting from this work are relatively in good agreement with the

Table 4. Mass absorption efficiency (MAE, $10^{-3} \text{ m}^2 \text{ g}^{-1}$) and Ångström absorption exponent (AAE) in the $\text{PM}_{10.6}$ and $\text{PM}_{2.5}$ size fractions. Absolute errors are in parentheses.

Geographical area	Sample	375 nm	407 nm	532 nm	635 nm	850 nm	AAE
PM_{10.6}							
Sahara	Morocco	– (–)	– (–)	– (–)	– (–)	– (–)	– (–)
	Libya	89 (11)	75 (9)	30 (5)	– (–)	– (–)	3.2 (0.3)
	Algeria	99 (10)	80 (10)	46 (7)	16 (3)	15 (3)	2.5 (0.3)
Sahel	Mali	– (–)	103 (18)	46 (12)	– (–)	– (–)	– (–)
	Bodélé	37 (4)	25 (3)	13 (2)	6 (1)	3 (1)	3.3 (0.3)
Middle East	Saudi Arabia	90 (9)	79 (9)	28 (3)	6 (1)	4 (1)	4.1 (0.4)
	Kuwait	– (–)	– (–)	– (–)	– (–)	– (–)	2.8 (0.3)
Southern Africa	Namibia	52 (7)	49 (7)	13 (3)	5 (2)	1 (2)	4.7 (0.5)
Eastern Asia	China	65 (9)	58 (7)	32 (4)	8 (2)	7 (2)	3 (0.3)
North America	Arizona	130 (15)	99 (12)	47 (7)	21 (4)	13 (4)	3.1 (0.3)
South America	Patagonia	102 (11)	80 (9)	29 (4)	17 (2)	10 (2)	2.9 (0.3)
Australia	Australia	135 (15)	121 (13)	55 (7)	26 (4)	14 (4)	2.9 (0.3)
PM_{2.5}							
Sahara	Morocco	107 (13)	88 (11)	34 (6)	14 (3)	15 (4)	2.6 (0.3)
	Libya	132(17)	103 (14)	33 (7)	– (–)	– (–)	4.1 (0.4)
	Algeria	95(9)	71 (11)	37 (7)	12 (5)	12 (5)	2.8 (0.3)
Sahel	Mali	711 (141)	621 (124)	227 (78)	– (–)	– (–)	3.4 (0.3)
	Bodelé	– (–)	– (–)	– (–)	– (–)	– (–)	– (–)
Middle East	Saudi Arabia	153 (18)	127 (15)	42 (7)	8 (4)	6 (4)	4.5 (0.5)
	Kuwait	270 (100)	324 (96)	– (–)	54 (52)	– (–)	3.4 (0.3)
Southern Africa	Namibia	147 (36)	131 (32)	31 (21)	6 (16)	3 (15)	5.1 (0.5)
Eastern Asia	China	201 (30)	176 (26)	89 (17)	14 (10)	23 (10)	3.2 (0.3)
North America	Arizona	– (–)	– (–)	– (–)	– (–)	– (–)	– (–)
South America	Patagonia	– (–)	– (–)	– (–)	– (–)	– (–)	2.9 (0.3)
Australia	Australia	335 (39)	288 (33)	130 (19)	57 (11)	36 (9)	2.9 (0.3)

estimates available in the literature (Alfaro et al., 2004; Linke et al., 2006; Yang et al., 2009; Denjean et al., 2016b), reported in Table 5. For the China Ulah Buhn sample, Alfaro et al. (2004) reported 69.1×10^{-3} and $9.8 \times 10^{-3} \text{ m}^2 \text{ g}^{-1}$ at 325 and 660 nm, respectively. The former is lower than the value of $99 \times 10^{-3} \text{ m}^2 \text{ g}^{-1}$ that we obtain by extrapolating our measurement at 375 nm. Likewise, our values for the Morocco sample are higher than reported by Linke et al. (2006) at 266 and 660 nm. Conversely, the agreement with the estimates of Yang et al. (2009) for mineral dust locally re-suspended in Xianghe, near Beijing (China), is very good at all wavelengths between 375 and 880 nm. As expected, the MAE values for mineral dust resulting from this work are almost 1 order of magnitude smaller than for other absorbing aerosols. For black carbon, MAE values are in the range of $6.5\text{--}7.5 \text{ m}^2 \text{ g}^{-1}$ at 850 nm (Bond and

Bergstrom, 2006; Massabò et al., 2016) and decrease in a linear way with the logarithm of the wavelength. For brown carbon, the reported MAE range between 2.3 and $7.0 \text{ m}^2 \text{ g}^{-1}$ at 350 nm (Chen and Bond, 2010; Kirchstetter et al., 2004; Massabò et al., 2016), 0.05 and $1.2 \text{ m}^2 \text{ g}^{-1}$ at 440 nm (Wang et al., 2016) and 0.08 and $0.72 \text{ m}^2 \text{ g}^{-1}$ at 550 nm (Chen and Bond, 2010).

The analysis of Table 4 indicates that, at every wavelength, the MAE values in the $\text{PM}_{2.5}$ fraction are equal or higher than those for $\text{PM}_{10.6}$. The $\text{PM}_{2.5} / \text{PM}_{10.6}$ MAE ratios reach values of 6 for the Mali sample but are mostly in the range 1.5–3 for the other aerosols. The values decrease with wavelength up to 635 nm, whereas at 850 nm they have values comparable to those at 375 nm. The observed size dependence of the MAE values is consistent with the expected behavior of light absorption of particles in the Mie and geometric opti-

Table 5. Mass absorption efficiency (MAE, $10^{-3} \text{ m}^2 \text{ g}^{-1}$) and Ångström absorption exponent (AAE) from the literature data discussed in the paper.

Geographical area	Sample	266 nm	325 nm	428 nm	532 nm	660 nm	880 nm	1064 nm	AAE
Sahara	Morocco ^a								2.25–5.13
	Morocco, PM _{2.5} ^b								2.0–6.5
	Morocco, submicron ^c	1100			60			30	4.2
	Egypt, submicron ^c	810			20				5.3
	Tunisia ^d		83			11			
	Saharan, transported ^e								2.9 ± 0.2
	Saharan, transported (PM ₁₀) ^f			37	27 ^f	15 ^g			2.9
Sahel	Saharan, transported (PM ₁) ^f			60	40 ^g	30 ^h			2.0
	Niger ^d		124			19			
Eastern Asia	China ^d		69			10			
	China ⁱ		87 ^j	50 ^k	27 ^l	13	1		3.8
Arabian Peninsula, N/NE Africa, Central Asia	Various locations ^m								2.5–3.9

^a Müller et al. (2009). ^b Petzold et al. (2009). ^c Linke et al. (2006). ^d Alfaro et al. (2004). ^e Fialho et al. (2005). ^f Denjean et al. (2016b). ^g At 528 nm. ^h At 652 nm. ⁱ Yang et al. (2009). ^j At 375 nm. ^k At 470 nm. ^l At 590 nm. ^m Moosmüller et al. (2012).

cal regimes that are relevant for the two size fractions. Light absorption of particles of sizes smaller or equivalent to the wavelength is proportional to their bulk volume, whereas for larger particles absorption occurs on their surface only (Bohren and Huffman, 1983). In contrast, the size-resolved measurements of Lafon et al. (2006) show that the proportion (by volume) of iron oxides might be higher in the coarse than in the fine fraction, which would counteract the size-dependence behavior of MAE. To validate the observations, we calculated the spectrally resolved MAE values in the two size fractions using the Mie code for homogeneous spherical particles (Bohren and Huffman, 1983) and the number size distribution estimated by Di Biagio et al. (2017) and averaged over the duration of filter sampling. We estimated the dust complex refractive index as a volume-weighted average of a non-absorbing dust fraction having the refractive index of kaolinite, the dominant mineral in our samples (see Di Biagio et al., 2017), from Egan et Hilgeman (1979) and an absorbing fraction estimated from the mass fraction of iron oxides and having the refractive index of hematite (Bédidi and Cervelle, 1993). The results of this calculation indicate that the observed size-dependent behavior is well reproduced at all wavelengths, even in the basic hypothesis that the mineralogical composition does not change with size. The only exception is 850 nm, where at times the PM_{2.5} / PM_{10.6} MAE ratio is much higher than expected theoretically. We attribute that to the relatively high uncertainty affecting the absorbance measurements at this wavelength, where the signal-to-noise ratio is low. Indeed, the two sets of values (MAE in the PM_{2.5} fraction and MAE in the PM_{10.6} fraction) are not statistically different according to a two-pair *t* test (0.01 and

0.05 level of confidence), confirming that any attempt of differentiation of the size dependence at this wavelength would require a stronger optical signal.

The analysis of the spectral dependence, using the power-law function fit (Eq. 2), provides the values of the AAE, also reported in Table 4. Contrary to the MAE values, there is no statistically significant size dependence of the AAE values, ranging from 2.5 (± 0.2) to 4.1 (± 0.3), with an average of 3.3 (± 0.7), for the PM_{10.6} size fraction and between 2.6 (± 0.2) and 5.1 (± 0.4), with an average of 3.5 (± 0.8), for the PM_{2.5} fraction. Our values are in the range of those published in the literature (Fialho et al., 2005; Linke et al., 2006; Müller et al., 2009; Petzold et al., 2009; Yang et al., 2009; Weinzierl et al., 2011; Moosmüller et al., 2012; Denjean et al., 2016b), shown in Table 5. AAE values close to 1.0 are found for urban aerosols where fossil fuel combustion is dominant, while AAE values for brown carbon from incomplete combustion are in the range of 3.5–4.2 (Yang et al., 2009; Chen et al., 2015; Massabò et al., 2016).

Finally, Fig. 4 shows correlations between the MAE values in the PM_{10.6} fraction (Fig. 4a) and in the PM_{2.5} fraction (Fig. 4b) and the estimated percent mass fraction of iron and iron oxides (MC_{Fe%} and MC_{Fe ox%}), respectively. Regardless of the size fraction, the correlation between the MAE values and the percent mass of total elemental iron are higher at 375, 407 and 532 nm. Best correlations are obtained when forcing the intercept to zero, indicating that elemental iron fully accounts for the measured absorption. At these wavelengths, linear correlations with the mass fraction of iron oxides are low in the PM_{10.6} mass fraction (R^2 up to 0.38–0.62) but higher in the PM_{2.5} fraction (R^2 up to 0.83–0.99), where,

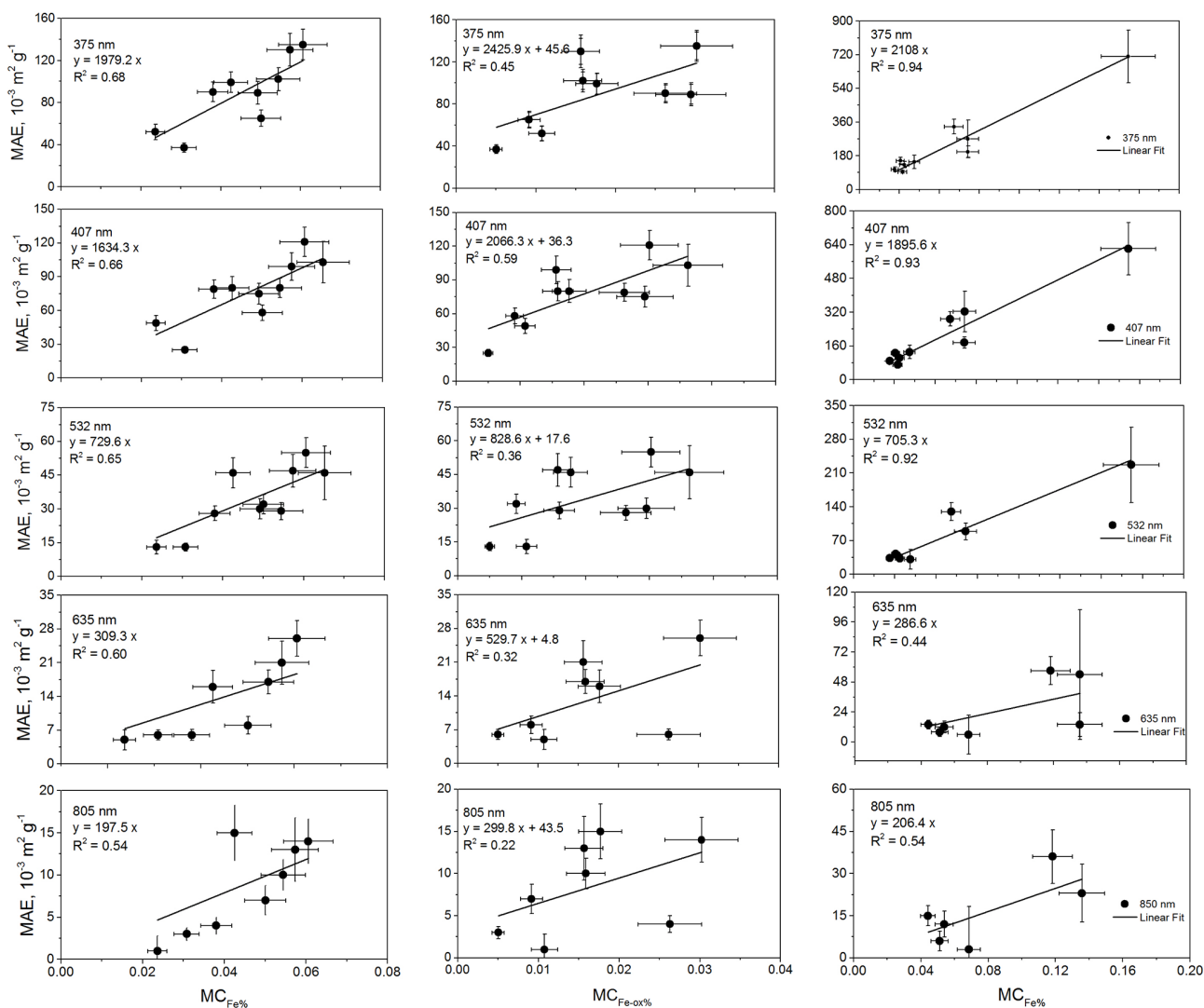


Figure 4. Illustration of the links between the MAE values and the dust chemical composition found in this study. Left column panels, from top to bottom: linear regression between the MAE values in the range from 375 to 850 nm and the fraction of elemental iron relative to the total dust mass ($\text{MR}_{\text{Fe}\%}$) in the $\text{PM}_{10.6}$ fraction; middle column panels: same as left column panels but for the mass fraction of iron oxides relative to the total dust mass ($\text{MR}_{\text{Fe-ox}\%}$) in the $\text{PM}_{10.6}$ size fraction; right column panels: same as left column panels but in the $\text{PM}_{2.5}$ size fraction.

however, one should keep in mind that they have been established only indirectly by considering the ratio of iron oxides to elemental iron independent of size. At 660 and 850 nm, little or no robust correlations are obtained, often based on very few data points and with very low MAE values. It is noteworthy that, in both size fractions, the linear correlation yields a nonzero intercept, indicating a contribution from minerals other than iron oxides to the measured absorption.

5 Conclusive remarks

In this paper, we report new laboratory measurements of the shortwave MAE of mineral dust of different origins and as

a function of size and wavelength in the 375–850 nm range. Our results were obtained in the CESAM using mineral dust generated from natural parent soils, in combination with optical and gravimetric analysis on extracted samples.

Our results can be summarized as follows: at 375 nm, the MAE values are lower for the $\text{PM}_{10.6}$ mass fraction (range $37\text{--}135 \times 10^{-3} \text{ m}^2 \text{ g}^{-1}$) than for the $\text{PM}_{2.5}$ fraction (range $95\text{--}711 \times 10^{-3} \text{ m}^2 \text{ g}^{-1}$), and they vary opposite to wavelength as $\lambda^{-\text{AAE}}$, where AAE averages between 3.3 and 3.5 regardless of size fraction. These results deserve some concluding comments:

- The size dependence, characterized by significantly higher MAE values in the fine fraction ($\text{PM}_{2.5}$) than in

the bulk (PM_{10.6}) aerosol, indicates that light absorption by mineral dust can be important even during atmospheric transport over heavily polluted regions, where dust concentrations are significantly lower than at emission. This can be shown by comparing the aerosol absorption optical depth (AAOD) at 440 nm for China, a well-known mixing region of mineral dust and pollution (e.g., Yang et al., 2009; Laskin et al., 2014), as well as offshore western Africa where large urban centers are downwind of dust transport areas (Petzold et al., 2011). Laskin et al. (2014) report that the average AAOD in China is of the order of 0.1 for carbonaceous absorbing aerosols (sum of black and brown carbon; Andreae and Gelencsér, 2006). This is lower or comparable to the AAOD of 0.17 and 0.11 at 407 nm (total and fine mass fractions, respectively) that we derive by a simple calculation ($AAOD = MAE \times MC_{dust} \times H$) from MAE values estimated in this study; MC_{dust} , the dust mass concentrations typically observed in urban Beijing during dust storms (Sun et al., 2005); and H , a scale height factor of 1 km.

- The spectral variability of the dust MAE values, represented by the AAE parameter, is equal in the PM_{2.5} and PM_{10.6} mass fractions. This suggests that, for a given size distribution, the possible variation of dust composition with size does not affect in a significant way the spectral behavior of the absorption properties. Our average value for AAE is 3.3 ± 0.7 , higher than for black carbon, but in the same range as light-absorbing organic (brown) carbon. As a result, depending on the environment, there can be some ambiguity in apportioning the AAOD based on spectral dependence. Bahadur et al. (2012) and Chung et al. (2012) couple the AAE and the spectral dependence of the total AOD (and/or its scattering fraction only) to overcome this problem. Still, Bahadur et al. (2012) show that there is an overlap in the scatterplots of the spectral dependence of the scattering and absorption fractions of the AOD based on an analysis of ground-based remote-sensing data for mineral dust, urban and non-urban fossil fuel over California. A closer look should be taken at observations in mixing areas where biomass burning aerosols may have different chemical composition and/or mineral dust has heavy loadings in order to generalize the clear separation observed in the spectral dependences of mineral dust and biomass burning (Bahadur et al., 2012). This aspect is relevant to the development of remote-sensing retrievals of light absorption by aerosols from space and their assimilation in climate models (Torres et al., 2007; Buchard et al., 2015; Hammer et al., 2016).
- There is an important sample-to-sample variability in our dataset of MAE values for mineral dust aerosols. At 532 nm, our average MAE values are 34 ± 14 and $78 \pm 70 \text{ m}^2 \text{ g}^{-1}$ in the PM_{10.6} and PM_{2.5} mass fractions,

respectively. Figure 3, showing the correlation with the estimated mass fraction of elemental iron and iron oxides, suggests that this variability could be related to the regional differences of the mineralogical composition of the parent soils. These observations lead to further conclusions. To start with, our study reinforces the need for regionally resolved representation of the light-absorption properties of mineral dust in order to improve the representation of its effect on climate. As a matter of fact, the natural variability of the absorption properties that we obtain from our study is in the range 50–100 %, even when we limit ourselves to smaller spatial scales, for example those from northern Africa (samples from Libya, Algeria, Mali and Bodélé). As a comparison, Solmon et al. (2008) showed that varying the single scattering albedo of mineral dust over western Africa by ± 5 %, that is, varying the co-albedo (or absorption) by 45 % (0.1 ± 0.045), could drastically change the climate response in the region.

The question is then “how to represent this regional variability?” Like Moosmüller et al. (2012) and Engelbrecht et al. (2016), we found that elemental iron is a very good proxy for the MAE, especially in the PM_{2.5} fraction, where iron-bearing absorbing minerals (hematite, goethite, illite, smectite clays) are more concentrated. In the coarse fraction, Ca-rich minerals, quartz and feldspars could also play a role, and that could result in the observed lower correlation (although adding a term proportional to elemental Ca does not improve the correlation in the present study). The correlation of the spectral MAE values with the iron oxide fraction is satisfactory but rather noisy, also owing to some uncertainty in the quantification of iron oxides from X-ray absorption measurements. In this case, the intercept is significantly different from zero, again indicating that a small but distinct fraction of absorption is due to minerals other than iron oxides. There are contrasting results on this topic: Alfaro et al. (2004) found an excellent correlation between MAE and the iron oxide content, whereas Klaver et al. (2011) found that the single scattering albedo (representing the capacity of an aerosol population to absorb light in relation to extinction) was almost independent on the mass fraction of iron oxides. Moosmüller et al. (2012) disagreed, pointing out the uncertainty in the correction procedure of the measurement of absorption by Klaver et al. (2011). As a matter of fact, Klaver et al. (2011) and Alfaro et al. (2004) used the same correction procedure. It is more likely that the lack of correlation found in Klaver et al. (2011) is due to the fact that minerals other than iron oxides contribute to absorption, in particular at their working wavelength (567 nm), where the absorption efficiency of iron oxides starts to weaken. Clearly, the linear correlation between elemental iron in mineral dust

and its light-absorption properties could ease the application and validation of climate models that are now starting to include the representation of the mineralogy (Perlwitz et al., 2015a, b; Scanza et al., 2015). Also, this would facilitate detecting source regions based on remote sensing of dust absorption in the UV–vis spectral region (e.g., Hsu et al., 2004). However, such a quantitative relationship cannot be uniquely determined from these studies, including the present one, which use different ways of estimating elemental iron, iron oxides and the total dust mass. A more robust estimate should be obtained from the imaginary parts of the complex refractive indices associated with the measurements of absorption and their dependence on the mineralogical composition.

Data availability. Experimental and processed data are immediately available upon request to the contact author. They will also soon be made available through the EROCHAMP-2020 data center.

The Supplement related to this article is available online at <https://doi.org/10.5194/acp-17-7175-2017-supplement>.

Author contributions. Lorenzo Caponi, Paola Formenti, Dario Massabò, Paolo Prati, Claudia Di Biagio and Jean-François Doussin designed the chamber experiments and discussed the results. Lorenzo Caponi and Claudia Di Biagio conducted the experiments with contributions by Mathieu Cazaunau, Edouard Pangui, Paola Formenti and Jean-François Doussin. Lorenzo Caponi, Dario Massabò and Paola Formenti performed the full data analysis with contributions by Claudia Di Biagio, Paolo Prati and Jean-François Doussin. Lorenzo Caponi, Paola Formenti and Servanne Chevaillier performed the XRF measurements. Paola Formenti and Gautier Landrot performed the XAS measurements. Dario Massabò performed the MWAA and the gravimetric measurements. Meinrat O. Andreae, Konrad Kandler, Thuraya Saeed, Stuart Piketh, Dave Seibert and Earle Williams collected the soil samples used for experiments. Lorenzo Caponi, Paola Formenti, Dario Massabò and Paolo Prati wrote the manuscript with comments from all co-authors.

Competing interests. The authors declare that they have no conflict of interest.

Acknowledgements. This work has received funding from the European Union's Horizon 2020 research and innovation programme through the EUROCHAMP-2020 Infrastructure Activity under grant agreement no. 730997. It was supported by the French national programme LEFE/INSU, by the OSU-EFLUVE (Observatoire des Sciences de l'Univers-Enveloppes Fluides de la Ville à l'Exobiologie) through dedicated research funding, by the CNRS-INSU by supporting CESAM as national facility and by the project of the TOSCA program of the CNES (Centre National

des Études Spatiales). Claudia Di Biagio was supported by the CNRS via the Labex L-IPSL. Meinrat O. Andreae was supported by funding from King Saud University and the Max Planck Society. The mobility of researchers between Italy and France was supported by the PICS programme MedMex of the CNRS-INSU. The authors acknowledge the CNRS-INSU for supporting CESAM as a national facility. Konrad Kandler acknowledges support from the Deutsche Forschungsgemeinschaft (DFG grant KA 2280/2-1). The authors strongly thank the LISA staff who participated in the collection of the soil samples from Patagonia and the Gobi used in this study and the two anonymous reviewers for useful comments on the manuscript. Paola Formenti thanks Hans Moosmüller (Desert Research Institute, Reno, Nevada) for providing fruitful suggestions for improvement and discussion to the paper.

Edited by: T. Takemura

Reviewed by: two anonymous referees

References

- Alfaro, S. C., Lafon, S., Rajot, J. L., Formenti, P., Gaudichet, A., and Maille, M.: Iron oxides and light absorption by pure desert dust: An experimental study, *J. Geophys. Res.-Atmos.*, 109, D08208, <https://doi.org/10.1029/2003JD004374>, 2004.
- Andreae, M. O. and Gelencsér, A.: Black carbon or brown carbon? The nature of light-absorbing carbonaceous aerosols, *Atmos. Chem. Phys.*, 6, 3131–3148, <https://doi.org/10.5194/acp-6-3131-2006>, 2006.
- Bahadur, R., Praveen, P. S., Xu, Y., and Ramanathan, V.: Solar absorption by elemental and brown carbon determined from spectral observations, *P. Natl. Acad. Sci. USA*, 109, 17366–17371, 2012.
- Balkanski, Y., Schulz, M., Claquin, T., and Guibert, S.: Re-evaluation of Mineral aerosol radiative forcing suggests a better agreement with satellite and AERONET data, *Atmos. Chem. Phys.*, 7, 81–95, <https://doi.org/10.5194/acp-7-81-2007>.
- Bédidi, A. and Cervelle B.: Light scattering by spherical particles with hematite and goethitelike optical properties: Effect of water impregnation, *J. Geophys. Res.*, 98, 11941–11952, <https://doi.org/10.1029/93JB00188>, 1993.
- Bohren, C. F. and Huffman, D. R.: *Absorption and scattering of light by small particles*, Wiley, New York, 1983.
- Bond, T. C. and Bergstrom, R. W.: Light absorption by carbonaceous particles: an investigative review, *Aerosol Sci. Tech.*, 40, 27–67, 2006.
- Boucher, O., Randall, D., Artaxo, P., Bretherton, C., Feingold, G., Forster, P., Kerminen, V.-M., Kondo, Y., Liao, H., Lohmann, U., Rasch, P., Satheesh, S.K., Sherwood, S., Stevens B., and Zhang, X. Y.: Clouds and Aerosols, in: *Climate Change 2013: The Physical Science Basis*, Contribution of Working Group I to the Fifth Assessment Report of the Intergovernmental Panel on Climate Change, edited by: Stocker, T. F., Qin, D., Plattner, G.-K., Tignor, M., Allen, S. K., Boschung, J., Nauels, A., Xia, Y., Bex, V., and Midgley, P. M., Cambridge University Press, Cambridge, UK and New York, NY, USA, 2013.
- Brégonzio-Rozier, L., Siekmann, F., Giorio, C., Pangui, E., Morales, S. B., Temime-Roussel, B., Gratien, A., Michoud, V., Ravier, S., Cazaunau, M., Tapparo, A., Monod, A., and Doussin,

- J.-F.: Gaseous products and secondary organic aerosol formation during long term oxidation of isoprene and methacrolein, *Atmos. Chem. Phys.*, 15, 2953–2968, <https://doi.org/10.5194/acp-15-2953-2015>, 2015.
- Brégonzio-Rozier, L., Giorio, C., Siekmann, F., Pangui, E., Morales, S. B., Temime-Roussel, B., Gratien, A., Michoud, V., Cazaunau, M., DeWitt, H. L., Tapparo, A., Monod, A., and Doussin, J.-F.: Secondary organic aerosol formation from isoprene photooxidation during cloud condensation–evaporation cycles, *Atmos. Chem. Phys.*, 16, 1747–1760, <https://doi.org/10.5194/acp-16-1747-2016>, 2016.
- Briois, V., Fonda, E., Belin, S., Barthe, L., La Fontaine, C., Langlois, F., Ribbens, M., and Villain, F.: UVX 2010 – 10e Colloque sur les Sources Cohérentes et Incohérentes UV, VUV et X, in: Applications et Développements Récents, EDP-Sciences, Les Ulis, 41–47, 2011.
- Bristow, C. S., Hudson-Edwards, K. A., and Chappell, A.: Fertilizing the Amazon and equatorial Atlantic with West African dust, *Geophys. Res. Lett.*, 37, L14807, <https://doi.org/10.1029/2010GL043486>, 2010.
- Buchard, V., da Silva, A. M., Colarco, P. R., Darmenov, A., Randles, C. A., Govindaraju, R., Torres, O., Campbell, J., and Spurr, R.: Using the OMI aerosol index and absorption aerosol optical depth to evaluate the NASA MERRA Aerosol Reanalysis, *Atmos. Chem. Phys.*, 15, 5743–5760, <https://doi.org/10.5194/acp-15-5743-2015>, 2015.
- Chen, L.-W. A., Chow, J. C., Wang, X. L., Robles, J. A., Sumlin, B. J., Lowenthal, D. H., Zimmermann, R., and Watson, J. G.: Multi-wavelength optical measurement to enhance thermal/optical analysis for carbonaceous aerosol, *Atmos. Meas. Tech.*, 8, 451–461, <https://doi.org/10.5194/amt-8-451-2015>, 2015.
- Chen, Y. and Bond, T. C.: Light absorption by organic carbon from wood combustion, *Atmos. Chem. Phys.*, 10, 1773–1787, <https://doi.org/10.5194/acp-10-1773-2010>, 2010.
- Chiapello, I.: Dust Observations and Climatology, in: *Mineral Dust: A Key Player in the Earth System*, edited by: Knippertz, P. and Stuut, J.-B. W., Springer Science & Business Media, Dordrecht, https://doi.org/10.1007/978-94-017-8978-3_7, 2014.
- Chiapello, I., Bergametti, G., Chatenet, B., Bousquet, P., Dulac, F., and Santos Suarez, E.: Origins of African dust transported over the northeastern tropical Atlantic, *J. Geophys. Res.*, 102, 13701–13709, 1997.
- Chung, C. E., Ramanathan, V., and Decremer, D.: Observationally constrained estimates of carbonaceous aerosol radiative forcing, *P. Natl. Acad. Sci. USA*, 109, 11624–11629, 2012.
- Coakley, J. A. and Chylek, P.: The two-stream approximation in radiative transfer: Including the angle of incident radiation, *J. Atmos. Sci.*, 32, 409–418, 1975.
- Colarco, P. R., Toon, O. B., Torres, O., and Rasch, F. J.: Determining the UV imaginary part of refractive index of Saharan dust particles from TOMS data and a three dimensional model of dust transport, *J. Geophys. Res.*, 107, 4289–4307, <https://doi.org/10.1029/2001JD000903>, 2002.
- Cornille, P., Maenhaut, W., and Pacyna, J. M.: Sources and characteristics of the atmospheric aerosol near Damascus, Syria, *Atmo. Environ. A*, 24, 1083–1093, 1990.
- Denjean, C., Formenti, P., Picquet-Varrault, B., Pangui, E., Zapf, P., Katrib, Y., Giorio, C., Tapparo, A., Monod, A., Temime-Roussel, B., Decorse, P., Mangeney, C., and Doussin, J. F.: Relating hygroscopicity and optical properties to chemical composition and structure of secondary organic aerosol particles generated from the ozonolysis of α -pinene, *Atmos. Chem. Phys.*, 15, 3339–3358, <https://doi.org/10.5194/acp-15-3339-2015>, 2015a.
- Denjean, C., Formenti, P., Picquet-Varrault, B., Camredon, M., Pangui, E., Zapf, P., Katrib, Y., Giorio, C., Tapparo, A., Temime-Roussel, B., Monod, A., Aumont, B., and Doussin, J. F.: Aging of secondary organic aerosol generated from the ozonolysis of α -pinene: effects of ozone, light and temperature, *Atmos. Chem. Phys.*, 15, 883–897, <https://doi.org/10.5194/acp-15-883-2015>, 2015b.
- Denjean, C., Cassola, F., Mazzino, A., Triquet, S., Chevillier, S., Grand, N., Bourriane, T., Momboisse, G., Selligri, K., Schwarzenbock, A., Freney, E., Mallet, M., and Formenti, P.: Size distribution and optical properties of mineral dust aerosols transported in the western Mediterranean, *Atmos. Chem. Phys.*, 16, 1081–1104, <https://doi.org/10.5194/acp-16-1081-2016>, 2016a.
- Denjean, C., Formenti, P., Desboeufs, K., Chevillier, S., Maillé, M., Cazaunau, M., Laurent, B., Mayol-Bracero, O. L., Vallejo, P., Quiñones, M., Gutierrez-Molina, I. E., Cassola, F., Prati, P., Andrews, E., and Ogren, J.: Size distribution and optical properties of African mineral dust after intercontinental transport, *J. Geophys. Res.-Atmos.*, 121, 7117–7138, <https://doi.org/10.1002/2016JD024783>, 2016b.
- Derimian, Y., Karnieli, A., Kaufman, Y. J., Andreae, M. O., Andreae, T. W., Dubovik, O., Maenhaut, W., and Koren, I.: The role of iron and black carbon in aerosol light absorption, *Atmos. Chem. Phys.*, 8, 3623–3637, <https://doi.org/10.5194/acp-8-3623-2008>, 2008.
- Di Biagio, C., Formenti, P., Styler, S. A., Pangui, E., and Doussin, J.-F.: Laboratory chamber measurements of the longwave extinction spectra and complex refractive indices of African and Asian mineral dusts, *Geophys. Res. Lett.*, 41, 6289–6297, <https://doi.org/10.1002/2014GL060213>, 2014.
- Di Biagio, C., Formenti, P., Balkanski, Y., Caponi, L., Cazaunau, M., Pangui, E., Journet, E., Nowak, S., Caqueneau, S., Andreae, M. O., Kandler, K., Saeed, T., Piketh, S., Seibert, D., Williams, E., and Doussin, J.-F.: Global scale variability of the mineral dust long-wave refractive index: a new dataset of in situ measurements for climate modeling and remote sensing, *Atmos. Chem. Phys.*, 17, 1901–1929, <https://doi.org/10.5194/acp-17-1901-2017>, 2017.
- di Sarra, A., Di Biagio, C., Meloni, D., Monteleone, F., Pace, G., Pugnaghi, S., and Sferlazzo, D.: Shortwave and longwave radiative effects of the intense Saharan dust event of March 25–26, 2010, at Lampedusa (Mediterranean sea), *J. Geophys. Res.*, 116, D23209, <https://doi.org/10.1029/2011JD016238>, 2011.
- Dubovik, O., Holben, B. N., Eck, T. F., Smirnov, A., Kaufman, Y. J., King, M. D., Tanre, D., and Slutsker, I.: Variability of absorption and optical properties of key aerosol types observed in worldwide locations, *J. Atmos. Sci.*, 59, 590–608, 2002.
- Egan, W. G. and Hilgeman, T. W.: *Optical Properties of Inhomogeneous Materials: Applications to Geology*, in: *Astronomy, Chemistry, and Engineering*, Academic Press, New York, NY, 235 pp., 1979.
- Engelbrecht, J. P., Moosmüller, H., Pincock, S., Jayanty, R. K. M., Lersch, T., and Casuccio, G.: Technical note: Mineralogical, chemical, morphological, and optical interrelationships of min-

- eral dust re-suspensions, *Atmos. Chem. Phys.*, 16, 10809–10830, <https://doi.org/10.5194/acp-16-10809-2016>, 2016.
- Fialho, P., Hansen, A. D. A., and Honrath, R. E.: Absorption coefficients by aerosols in remote areas: a new approach to decouple dust and black carbon absorption coefficients using seven-wavelength Aethalometer data, *J. Aerosol Sci.*, 36, 267–282, 2005.
- Formenti, P., Andreae, M. O., Lange, L., Roberts, G., Cafmeyer, J., Rajta, I., Maenhaut, W., Holben, B. N., Artaxo, P., and Lelieveld, J.: Saharan dust in Brazil and Suriname during the Large-Scale Biosphere–Atmosphere Experiment in Amazonia (LBA) – Cooperative LBA Regional Experiment (CLAIRE) in March 1998, *J. Geophys. Res.*, 106, 14919–14934, <https://doi.org/10.1029/2000jd900827>, 2001.
- Formenti, P., Nava, S., Prati, P., Chevaillier, S., Klaver, A., Lafon, S., Mazzei, F., Calzolari, G., and Chiari, M.: Self-attenuation artifacts and correction factors of light element measurements by X-ray analysis: Implication for mineral dust composition studies, *J. Geophys. Res.*, 115, D01203, <https://doi.org/10.1029/2009JD012701>, 2010.
- Formenti, P., Rajot, J. L., Desboeufs, K., Saïd, F., Grand, N., Chevaillier, S., and Schmechtig, C.: Airborne observations of mineral dust over western Africa in the summer Monsoon season: spatial and vertical variability of physico-chemical and optical properties, *Atmos. Chem. Phys.*, 11, 6387–6410, <https://doi.org/10.5194/acp-11-6387-2011>, 2011.
- Formenti, P., Caquineau, S., Desboeufs, K., Klaver, A., Chevaillier, S., Journet, E., and Rajot, J. L.: Mapping the physico-chemical properties of mineral dust in western Africa: mineralogical composition, *Atmos. Chem. Phys.*, 14, 10663–10686, <https://doi.org/10.5194/acp-14-10663-2014>, 2014a.
- Formenti, P., Caquineau, S., Chevaillier, S., Klaver, A., Desboeufs, K., Rajot, J. L., Belin, S., and Briois, V.: Dominance of goethite over hematite in iron oxides of mineral dust from western Africa: quantitative partitioning by X-ray Absorption Spectroscopy, *J. Geophys. Res.-Atmos.*, 119, 12740–12754, <https://doi.org/10.1002/2014JD021668>, 2014b.
- Hammer, M. S., Martin, R. V., van Donkelaar, A., Buchard, V., Torres, O., Ridley, D. A., and Spurr, R. J. D.: Interpreting the ultraviolet aerosol index observed with the OMI satellite instrument to understand absorption by organic aerosols: implications for atmospheric oxidation and direct radiative effects, *Atmos. Chem. Phys.*, 16, 2507–2523, <https://doi.org/10.5194/acp-16-2507-2016>, 2016.
- Hänel, G.: Radiation budget of the boundary layer: Part II. Simultaneous measurement of mean solar volume absorption and extinction coefficients of particles, *Beitr. Phys. Atmos.*, 60, 241–247, 1987.
- Hänel, G.: Optical properties of atmospheric particles: complete parameter sets obtained through polar photometry and an improved inversion technique, *Appl. Optics*, 33, 7187–7199, 1994.
- Haywood, J. M., Francis, P. N., Glew, M. D., and Taylor, J. P.: Optical properties and direct radiative effect of Saharan dust: A case study of two Saharan outbreaks using data from the U.K. Met. Office C-130, *J. Geophys. Res.*, 106, 18417–18430, 2001.
- Highwood, E. J. and Ryder, C. L.: Radiative Effects of Dust, in: *Mineral Dust: A Key Player in the Earth System*, edited by: Knippertz, P. and Stuut, J.-B. W., Springer Science + Business Media, Dordrecht, https://doi.org/10.1007/978-94-017-8978-3_11, 2014.
- Haywood, J., Francis, P., Osborne, S., Glew, M., Loeb, N., Highwood, E., Tanré, D., Myhre, G., Formenti, P., and Hirst, E.: Radiative properties and direct radiative effect of Saharan dust measured by the C-130 aircraft during Saharan Dust Experiment (SHADE). 1: Solar spectrum, *J. Geophys. Res.*, 108, 8577, <https://doi.org/10.1029/2002JD002687>, 2003.
- Hsu, N. C., Tsay, S.-C., King, M. D., and Herman, J. R.: Aerosol Properties Over Bright-Reflecting Source Regions, *IEEE T. Geosci. Remote*, 42, 557–569, 2004.
- Journet, E., Balkanski, Y., and Harrison, S. P.: A new data set of soil mineralogy for dust-cycle modeling, *Atmos. Chem. Phys.*, 14, 3801–3816, <https://doi.org/10.5194/acp-14-3801-2014>, 2014.
- Kandler, K., Benker, N., Bundke, U., Cuevas, E., Ebert, M., Knippertz, P., Rodríguez, S., Schütz, L., and Weinbruch, S.: Chemical composition and complex refractive index of Saharan Mineral Dust at Izaña, Tenerife (Spain) derived by elec-tron microscopy, *Atmos. Environ.*, 41, 8058–8074, <https://doi.org/10.1016/j.atmosenv.2007.06.047>, 2007.
- Kandler, K., Schütz, L., Deutscher, C., Hofmann, H., Jäckel, S., Knippertz, P., Lieke, K., Massling, A., Schladitz, A., Weinzierl, B., Zorn, S., Ebert, M., Jaenicke, R., Petzold, A., and Weinbruch, S.: Size distribution, mass concentration, chemical and mineralogical composition, and derived optical parameters of the boundary layer aerosol at Tinfou, Morocco, during SAMUM 2006, *Tellus B*, 61, 32–50, <https://doi.org/10.1111/j.1600-0889.2008.00385.x>, 2009.
- Kandler, K., Lieke, K., Benker, N., Emmel, C., Küpper, M., Müller-Ebert, D., Ebert, M., Scheuvsens, D., Schladitz, A., Schütz, L., and Weinbruch, S.: Electron microscopy of particles collected at Praia, Cape Verde, during the Saharan Mineral dust experiment: particle chemistry, shape, mixing state and complex refractive index, *Tellus B*, 63, 475–496, <https://doi.org/10.1111/j.1600-0889.2011.00550.x>, 2011.
- Karickhoff, S. W. and Bailey, G. W.: Optical absorption spectra of clay minerals, *Clays Clay Min.*, 21, 59–70, 1973.
- Kirchstetter, T. W., Novakok, T., and Hobbs, P. V.: Evidence that the spectral dependence of light absorption by aerosols is affected by organic carbon, *J. Geophys. Res.*, 109, D21208, <https://doi.org/10.1029/2004JD004999>, 2004.
- Klaver, A., Formenti, P., Caquineau, S., Chevaillier, S., Ausset, P., Calzolari, G., Osborne, S., Johnson, B., Harrison, M., and Dubovik, O.: Physico-chemical and optical properties of Sahelian and Saharan mineral dust: in situ measurements during the GERBILS campaign, *Q. J. Roy. Meteorol. Soc.*, 137, 1193–1210, <https://doi.org/10.1002/qj.889>, 2011.
- Knippertz, P. and Stuut, J.-B. W. (Eds.): *Mineral Dust: A Key Player in the Earth System*, Springer Science & Business Media, Dordrecht, https://doi.org/10.1007/978-94-017-8978-3_1, 2014.
- Lafon, S., Rajot, J., Alfaro, S., and Gaudichet, A.: Quantification of iron oxides in desert aerosol, *Atmos. Environ.*, 38, 1211–1218, 2004.
- Lafon, S., Sokolik, I. N., Rajot, J. L., Caquineau, S., and Gaudichet, A.: Characterization of iron oxides in mineral dust aerosols: Implications for light absorption, *J. Geophys. Res.*, 111, D21207, <https://doi.org/10.1029/2005JD007016>, 2006.
- Laskin, J., Laskin, A., Nizkorodov, S. A., Roach, P., Eckert, P., Gilles, M. K., Wang, B., Lee, H. J., and Hu, Q.: Molecular Selec-

- tivity of Brown Carbon Chromophores, *Environ. Sci. Technol.*, 48, 12047–12055, 2014.
- Lau, K. M., Kim, K. M., Sud, Y. C., and Walker, G. K.: A GCM study of the response of the atmospheric water cycle of West Africa and the Atlantic to Saharan dust radiative forcing, *Ann. Geophys.*, 27, 4023–4037, <https://doi.org/10.5194/angeo-27-4023-2009>, 2009.
- Lazaro, F. J., Gutiérrez, L., Barrón, V., and Gelado, M. D.: The speciation of iron in desert dust collected in Gran Canaria (Canary Islands): Combined chemical, magnetic and optical analysis, *Atmos. Environ.*, 42, 8987–8996, 2008.
- Lide, D. R.: *CRC Handbook of Chemistry and Physics 1991–1992*, CRC Press, Boca Raton, Florida, 1992.
- Linke, C., Möhler, O., Veres, A., Mohácsi, Á., Bozóki, Z., Szabó, G., and Schnaiter, M.: Optical properties and mineralogical composition of different Saharan mineral dust samples: a laboratory study, *Atmos. Chem. Phys.*, 6, 3315–3323, <https://doi.org/10.5194/acp-6-3315-2006>, 2006.
- Loeb, N. G. and Su, W.: Direct Aerosol Radiative Forcing Uncertainty Based on a Radiative Perturbation Analysis, *J. Climate*, 23, 5288–5293, 2010.
- Massabó, D., Bernardoni, V., Bove, M. C., Brunengo, A., Cuccia, E., Piazzalunga, A., Prati, P., Valli, G., and Vecchi, R.: A multi-wavelength optical set-up for the characterization of carbonaceous particulate matter, *J. Aerosol Sci.*, 60, 34–46, 2013.
- Massabó, D., Caponi, L., Bernardoni, V., Bove, M. C., Brotto, P., Calzolari, G., Cassola, F., Chiari, M., Fedi, M. E., Fermo, P., Giannoni, M., Lucarelli, F., Nava, S., Piazzalunga, A., Valli, G., Vecchi, R., and Prati, P.: Multi-wavelength optical determination of black and brown carbon in atmospheric aerosols, *Atmos. Environ.*, 108, 1–12, 2015.
- Massabó, D., Caponi, L., Bove, M. C., and Prati, P.: Brown carbon and thermal-optical analysis: A correction based on optical multi-wavelength apportionment of atmospheric aerosols, *Atmos. Environ.*, 125, 119–125, <https://doi.org/10.1016/j.atmosenv.2015.11.011>, 2016.
- McConnell, C. L., Highwood, E. J., Coe, H., Formenti, P., Anderson, B., Osborne, S., Nava, S., and Chen, G.: Seasonal variations of the physical and optical characteristics of Saharan dust: results from the Dust Outflow and Deposition to the Ocean (DODO) Experiment, *J. Geophys. Res.*, 113, D14S05, <https://doi.org/10.1029/2007JD009606>, 2008.
- Miller, R. L., Tegen, I., and Perlwitz, J. P.: Surface radiative forcing by soil dust aerosols and the hydrologic cycle, *J. Geophys. Res.*, 109, D04203, <https://doi.org/10.1029/2003JD004085>, 2004.
- Miller, R. L., Knippertz, P., Garcia-Pardo, C. P., Perlwitz, J. P., and Tegen, I.: Impact of dust radiative forcing upon climate, in: *Mineral Dust*, Springer Netherlands, 327–357, 2014.
- Ming, Y., Ramaswamy, V., and Persad, G.: Two opposing effects of absorbing aerosols on global mean precipitation, *Geophys. Res. Lett.*, 37, L13701, <https://doi.org/10.1029/2010GL042895>, 2010.
- Moosmüller, H., Chakrabarty, R. K., and Arnott, W. P.: Aerosol light absorption and its measurement: A review, *J. Quant. Spectrom. Ra.*, 110, 844–878, 2009.
- Moosmüller, H., Engelbrecht, J. P., Skiba, M., Frey, G., Chakrabarty, R. K., and Arnott, W. P.: Single scattering albedo of fine mineral dust aerosols controlled by iron concentration, *J. Geophys. Res.*, 117, D11210, <https://doi.org/10.1029/2011JD016909>, 2012.
- Moskowitz, B. M., Reynolds, R. L., Goldstein, H. L., Berquó, T. S., Kokaly, R. F., and Bristow, C. S.: Iron oxide minerals in dust-source sediments from the Bodélé Depression, Chad: Implications for radiative properties and Fe bioavailability of dust plumes from the Sahara, *Aeolian Res.*, 22, 93–106, 2016.
- Müller, T., Schladitz, A., Massling, A., Kaaden, N., Kandler, K., and Wiedensohler, A.: Spectral absorption coefficients and imaginary parts of refractive indices of Saharan dust during SAMUM-1, *Tellus B*, 61, 79–95, <https://doi.org/10.3402/tellusb.v61i1.16816>, 2009.
- Osborne, S. R., Johnson, B. T., Haywood, J. M., Baran, A. J., Harrison, M. A. J., and McConnell, C. L.: Physical and optical properties of mineral dust aerosol during the dust and biomass-burning experiment, *J. Geophys. Res.*, 113, D00C03, <https://doi.org/10.1029/2007JD009551>, 2008.
- Patterson, E. M., Gillette, D. A., and Stockton, B. H.: Complex index of refraction between 300 and 700 nm for Saharan aerosol, *J. Geophys. Res.*, 82, 3153–3160, 1977.
- Pérez C., Nickovic, S., Pejanovic, G., Baldasano, J. M., and Özsoy, E.: Interactive dust-radiation modeling: a step to improve weather forecasts, *J. Geophys. Res.*, 111, D16206, <https://doi.org/10.1029/2005JD006717>, 2006.
- Perlwitz, J. P. and Miller, R.: Cloud cover increase with increasing aerosol absorptivity – a counterexample to the conventional semi-direct aerosol effect, *J. Geophys. Res.*, 115, D08203, <https://doi.org/10.1029/2009JD012637>, 2010.
- Perlwitz, J. P., Pérez García-Pando, C., and Miller, R. L.: Predicting the mineral composition of dust aerosols – Part 1: Representing key processes, *Atmos. Chem. Phys.*, 15, 11593–11627, <https://doi.org/10.5194/acp-15-11593-2015>, 2015a.
- Perlwitz, J. P., Pérez García-Pando, C., and Miller, R. L.: Predicting the mineral composition of dust aerosols – Part 2: Model evaluation and identification of key processes with observations, *Atmos. Chem. Phys.*, 15, 11629–11652, <https://doi.org/10.5194/acp-15-11629-2015>, 2015b.
- Petzold, A. and Schönlinner, M.: Multi-angle absorption photometry – a new method for the measurement of aerosol light absorption and atmospheric black carbon, *J. Aerosol Sci.*, 35, 421–441, 2004.
- Petzold, A., Rasp, K., Weinzierl, B., Esselborn, M., Hamburger, T., Dornbrack, A., Kandler, K., Schütz, L., Knippertz, P., Fiebig, M., and Virkkula, A.: Saharan dust absorption and refractive index from aircraft-based observations during SAMUM 2006, *Tellus B*, 61, 118–130, 2009.
- Petzold, A., Veira, A., Mund, S., Esselborn, M., Kiemle, C., Weinzierl, B., Hamburger, T., Ehret, G., Lieke, K., and Kandler, K.: Mixing of mineral dust with urban pollution aerosol over Dakar (Senegal): impact on dust physico-chemical and radiative properties, *Tellus B*, 63, 619–634, <https://doi.org/10.1111/j.1600-0889.2011.00547.x>, 2011.
- Radhi, M., Box, M. A., Box, G. P., Mitchell, R. M., Cohen, D. D., Stelcer, E., and Keywood, M. D.: Size-resolved mass and chemical properties of dust aerosols from Australia's Lake Eyre Basin, *Atmos. Environ.*, 44, 3519–3528, <https://doi.org/10.1016/j.atmosenv.2010.06.016>, 2010.
- Radhi, M., Box, M. A., Box, G. P., Keywood, M. D., Cohen, D. D., Stelcer, E., and Mitchell, R. M.: Size-resolved chemical composition of Australian dust aerosol during winter, *Environ. Chem.*, 8, 248–262, 2011.

- Ravel, B. and Newville, M.: ATHENA, ARTEMIS, HEP-HAESTUS: data analysis for X-ray absorption spectroscopy using IFEFFIT, *J. Synchro. Ra.*, 12, 537–541, <https://doi.org/10.1107/S0909049505012719>, 2005.
- Reid, J. S., Flocchini, R. G., Cahill, T. A., Ruth, R. S., and Salgado, D. P.: Local meteorological, transport, and source aerosol characteristics of late autumn Owens Lake (dry) dust storms, *Atmos. Environ.*, 28, 1699–1706, [https://doi.org/10.1016/1352-2310\(94\)90315-8](https://doi.org/10.1016/1352-2310(94)90315-8), 1994.
- Ryder, C. L., Highwood, E. J., Rosenberg, P. D., Trembath, J., Brooke, J. K., Bart, M., Dean, A., Crosier, J., Dorsey, J., Brindley, H., Banks, J., Marsham, J. H., McQuaid, J. B., Sodemann, H., and Washington, R.: Optical properties of Saharan dust aerosol and contribution from the coarse mode as measured during the Fenec 2011 aircraft campaign, *Atmos. Chem. Phys.*, 13, 303–325, <https://doi.org/10.5194/acp-13-303-2013>, 2013a.
- Ryder, C. L., Highwood, E. J., Lai, T. M., Sodemann, H., and Marsham, J. H.: Impact of atmospheric transport on the evolution of microphysical and optical properties of Saharan dust, *Geophys. Res. Lett.*, 40, 2433–2438, <https://doi.org/10.1002/grl.50482>, 2013b.
- Scanza, R. A., Mahowald, N., Ghan, S., Zender, C. S., Kok, J. F., Liu, X., Zhang, Y., and Albani, S.: Modeling dust as component minerals in the Community Atmosphere Model: development of framework and impact on radiative forcing, *Atmos. Chem. Phys.*, 15, 537–561, <https://doi.org/10.5194/acp-15-537-2015>, 2015.
- Scheuven, D., Schütz, L., Kandler, K., Ebert, M., and Weinbruch, S.: Bulk composition of northern African dust and its source sediments – A compilation, *Earth-Sci. Rev.*, 116, 170–194, <https://doi.org/10.1016/j.earscirev.2012.08.005>, 2013.
- Shen, Z. X., Cao, J. J., Arimoto, R., Zhang, R. J., Jie, D. M., Liu, S. X., and Zhu, C. S.: Chemical composition and source characterization of spring aerosol over Horqin sand land in northeastern China, *J. Geophys. Res.*, 112, D14315, <https://doi.org/10.1029/2006JD007991>, 2007.
- Sinyuk, A., Torres, O., and Dubovik, O.: Combined use of satellite and surface observations to infer the imaginary part of refractive index of Saharan dust, *Geophys. Res. Lett.*, 30, 1081, <https://doi.org/10.1029/2002GL016189>, 2003.
- Slingo, A., Ackerman, T. P., Allan, R. P., Kassianov, E. I., McFarlane, S. A., Robinson, G. J., Barnard, J. C., Miller, M. A., Harries, J. E., Russell, J. E., and Dewitte, S.: Observations of the impact of a major Saharan dust storm on the atmospheric radiation balance, *Geophys. Res. Lett.*, 33, L24817, <https://doi.org/10.1029/2006GL027869>, 2006.
- Solmon, F., Mallet, M., Elguindi, N., Giorgi, F., Zaakey, A., and Konaré, A.: Dust aerosol impact on regional precipitation over western Africa, mechanisms and sensitivity to absorption properties, *Geophys. Res. Lett.*, 35, L24705, <https://doi.org/10.1029/2008GL035900>, 2008.
- Sun, Y., Zhuang, G., Wang, Y., Zhao, X., Li, J., Wang, Z., and An, Z.: Chemical composition of dust storms in Beijing and implications for the mixing of mineral aerosol with pollution aerosol on the pathway, *J. Geophys. Res.*, 110, D24209, <https://doi.org/10.1029/2005JD006054>, 2005.
- Tegen, I. and Lacis, A. A.: Modeling of particle size distribution and its influence on the radiative properties of mineral dust aerosol, *J. Geophys. Res.*, 101, 19237–19244, <https://doi.org/10.1029/95JD03610>, 1996.
- Torres, O., Tanskanen, A., Veihelmann, B., Ahn, C., Braak, R., Bhartia, P. K., Veefkind, P., and Levelt, P.: Aerosols and surface UV products from Ozone Monitoring Instrument observations: An overview, *J. Geophys. Res.*, 112, D24S47, <https://doi.org/10.1029/2007JD008809>, 2007.
- Utry, N., Ajtai, T., Filep, Á., Pintér, M., Tombacz, E., Bozóki, Z., and Szabó, G.: Correlations between absorption Ångström exponent (AAE) of wintertime ambient urban aerosol and its physical and chemical properties, *Atmos. Environ.*, 91, 52–59, 2014.
- Vinoj, V., Rasch, P. J., Wang, H., Yoon, J.-H., Ma, P.-L., Landu, K., and Singh, B.: Short-term modulation of Indian summer monsoon rainfall by West Asian dust, *Nat. Geosci.*, 7, 308–313, <https://doi.org/10.1038/ngeo2107>, 2014.
- Wagner, R., Ajtai, T., Kandler, K., Lieke, K., Linke, C., Müller, T., Schnaiter, M., and Vragel, M.: Complex refractive indices of Saharan dust samples at visible and near UV wavelengths: a laboratory study, *Atmos. Chem. Phys.*, 12, 2491–2512, <https://doi.org/10.5194/acp-12-2491-2012>, 2012.
- Wang, J., Doussin, J. F., Perrier, S., Perraudin, E., Katrib, Y., Pangu, E., and Picquet-Varrault, B.: Design of a new multi-phase experimental simulation chamber for atmospheric photochemistry and cloud chemistry research, *Atmos. Meas. Tech.*, 4, 2465–2494, <https://doi.org/10.5194/amt-4-2465-2011>, 2011.
- Wang, L., Li, Z., Tian, Q., Ma, Y., Zhang, F., Zhang, Y., Li, D., Li, K., and Li, L.: Estimate of aerosol absorbing components of black carbon, brown carbon, and dust from ground-based remote sensing data of sun-sky radiometers, *J. Geophys. Res.-Atmos.*, 118, 6534–6543, <https://doi.org/10.1002/jgrd.50356>, 2016.
- Weinzierl, B., Sauer, D., Esselborn, M., Petzold, A., Veira, A., Rose, M., Mund, S., Wirth, M., Ansmann, A., Tesche, M., Gross, S., and Freudenthaler, V.: Microphysical and optical properties of dust and tropical biomass burning aerosol layers in the Cape Verde region – an overview of the airborne in situ and lidar measurements during SAMUM-2, *Tellus B*, 63, 589–618, 2011.
- Xian, P.: Seasonal migration of the ITCZ and implications for aerosol radiative impact, PhD thesis, Columbia University, Columbia, 2008.
- Yang, M., Howell, S. G., Zhuang, J., and Huebert, B. J.: Attribution of aerosol light absorption to black carbon, brown carbon, and dust in China – interpretations of atmospheric measurements during EAST-AIRE, *Atmos. Chem. Phys.*, 9, 2035–2050, <https://doi.org/10.5194/acp-9-2035-2009>, 2009.
- Zhang, X. Y., Wang, Y. Q., Zhang, X. C., Guo, W., Niu, T., Gong, S. L., Yin, Y., Zhao, P., Jin, J. L., and Yu, M.: Aerosol monitoring at multiple locations in China: contributions of EC and dust to aerosol light absorption, *Tellus B*, 60, 647–656, 2008.
- Zhao, C., Liu, X., Ruby Leung, L., and Hagos, S.: Radiative impact of mineral dust on monsoon precipitation variability over West Africa, *Atmos. Chem. Phys.*, 11, 1879–1893, <https://doi.org/10.5194/acp-11-1879-2011>, 2011.